SCIENCE CHINA
Technological Sciences

December 2010 Vol.53 No.12: 3168–3174
doi: 10.1007/s11431-010-4160-8

Interface delamination of the thermal barrier coating subjected to local heating

WU ChenWu*, HUANG ChenGuang & CHEN GuangNan

Institute of Mechanics, Chinese Academy of Sciences, Beijing 100190, China

Received July 8, 2010; accepted September 16, 2010

To investigate the possible failure modes of the thermal barrier coating (TBC) used to protect the scramjet combustion chamber, the local heating via laser beam irradiation was utilized to simulate the service condition of high thermal flux and high temperature gradient. Firstly, the experimental method and process were described and the typical fracture morphology of the TBC under test were provided. Then, the theoretical and finite element modeling were carried out to study the temperature, deformation and stresses of the specimen when the top ceramic coat was subjected to local heating, and to demonstrate the mechanism on the failure of the TBC. It is revealed that the interface delamination shall appear and ultimately lead to the failure of the TBC under such thermal loading of local quick heating. According to the outcome of this study, the driving force of the interface delamination is influenced greatly by the key structural parameters and performance matching. Moreover, by utilizing the rules of the effects of these parameters on the fracture driving force, there is some possibility for the designer to optimize the performances of the TBC.

TBC, local heating, interface delamination, FE modeling

Citation: Wu C W, Huang C G, Chen G N. Interface delamination of the thermal barrier coating subjected to local heating. Sci China Tech Sci, 2010, 53: 3168–3174, doi: 10.1007/s11431-010-4160-8

1 Introduction

The scramjet is the heart of the hypersonic aerocraft, while the combustion chamber is the crucial part of the scramjet. To improve the thrust power of the fired gas, fuels are mixed and burnt in the combustion chamber with a decelerated air flow of increased pressure. It is expected to change as much as possible the chemical energy stored in the fuels into heat energy of the hot fired gas. As we all know, the thrust power of the fired gas is directly proportional to its temperature. So, the temperature of the fired gas in the combustion chamber is expected to be higher and higher to improve the thrust power and efficiency of the scramjet. Nowadays, the service temperature of the combustion chamber is even over 2500 K [1–3], which is too severe to be sustained by any sole structural material. Moreover, such severity should be enhanced with the increase of the service time of the scramjet, which requires reliable thermal protection for the combustion chamber. As a matter of fact, the technique of thermal protection in the combustion chamber has become one of the crucial technologies for the development of scramjet [2].

It is reported that the concept of utilizing both the active cooling and thermal barrier coatings is justified to be able to reduce the risk of thermal destruction of the combustion chamber structures [4–6]. For such thermal protective design, the thin panels are covered with thermal barrier coatings at the inner side and cooled by the cooling liquid flowing through the cooling groves at the outer side, adjacent to which are the thick panels acting as the mechanical loading parts. Generally, the distance from the cooling groove to the

*Corresponding author (email: chenwuwu@imech.ac.cn)

inner surface of the combustion chamber, i.e., the thickness of the thin panel is required to be as small as possible for a better cooling efficiency.

However, the high temperature gradient through the thin panel greatly challenges the performances of the thermal barrier coatings, which are commonly plated on the thin panel via plasma spraying [4]. Aiming at the reliability of such system of the thermal barrier coatings on the thin panel, a laboratory based test method was devised to realize the condition of high heat flux and high temperature gradient. The YAG laser was adopted to heat the top (ceramic) coat of the thermal barrier coatings and the cool water flow was utilized to cool the inner side of the thin panel. The experiments were carried out to investigate the possible failure modes of the thermal barrier coatings. Moreover, a mathematic-physical model of the experimental process was set up and the partial differential equations were solved by finite element method for the temperature, deformation and stresses. Finally, the mechanism on the experimentally observed fracture modes of the coatings were demonstrated and the influences of typical parameters on the reliability of the thermal barrier coatings were discussed.

2 Experimental description and results

During the preparation of the specimen for this study, the NiCrAlY bond coat of thickness 0.1 mm was deposited on the GH3128 substrate of thickness 1 mm before the 8% YSZ top coat of thickness 0.3 mm was plasma sprayed. The equipment for the experimental work are shown in Figures 1(a) and (b). The non-focalizing YAG laser of output power 100 W and beam diameter 6.5 mm was utilized to irradiate the top coat, of which the effective absorption coefficient was about 0.66 and the irradiation durations were in the range from 30–300 s. The initial temperature of the cooling water was 10°C and the intake pressure was about 0.2 MPa.

For almost all the local heating tests, interfacial crackings were observed between the top (ceramic) coat and the bond coat, which is known as interface delamination. The typical morphology of such interface delamination is shown in Figures 2(a) and (b), of which the former was obtained by optical microscopy (OM) and the latter by scanning electron microscopy (SEM). The interfacial crack could be found clearly between the top coat and the bond coat, which was further observed to be initiated at the center of the irradiated region and finally to lead to axis-symmetry interface separation.

From the point of view of continuum mechanics, the interfacial stresses induced by the deformation mismatch at the interface between the top coat and the bond coat are the direct driving forces for the initiation and propagation of the interface cracks or other interface defects. Such deformation mismatch at the interface owes both to the differeces in the thermo-mechnical performances such as thermal expansion

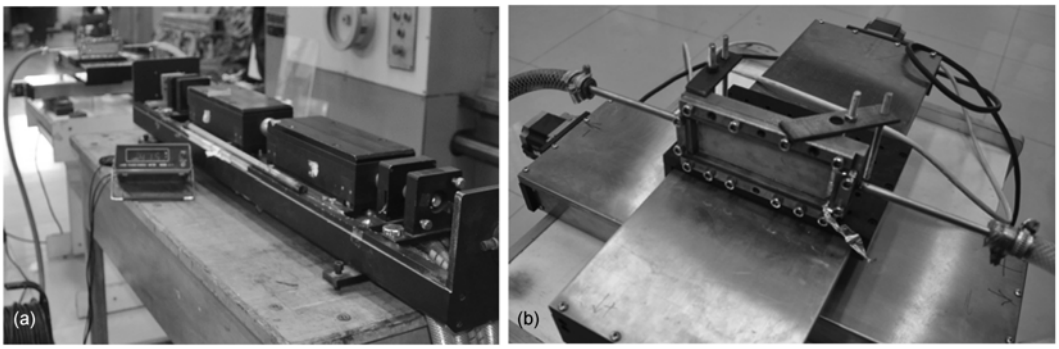

Figure 1 (a) the YAG laser and (b) the cooling equipment and specimen.

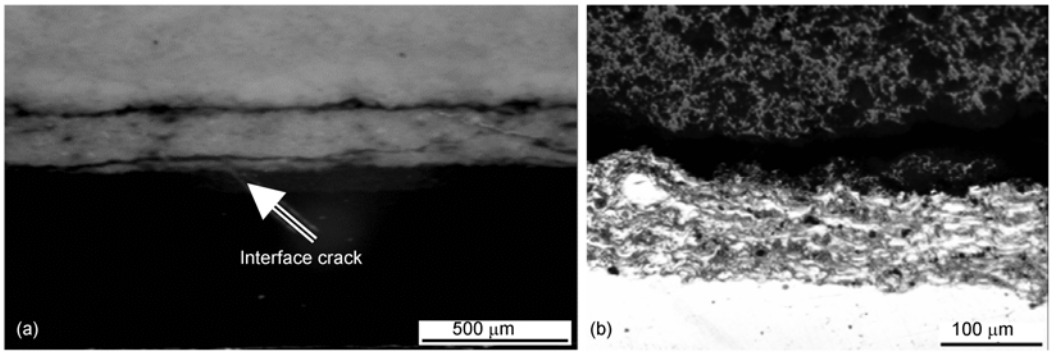

Figure 2 (a) OM photo and (b) SEM morphology of the interface delamination.

coefficients, elastic moduli and Poisson's ratio of the top coat and bond coat. What's more important, the high temperature gradients through the thickness of the specimen due to the coexistance of the local heating and flow cooling contributed greatly to the interface deformation mismatch. To describe the interface deformation mismatch and the interfacial stresses developed in the tested specimen, the continuum modeling of heat transfer and mechnics were set up and the transient temperature, deformation and stresses were computed numerically.

3 Theoretical analysis and numerical computation

3.1 Theoretical description of the thermo-mechanical responses to local heating

Considering the fact that the laser beam diameter is small enough in comparison with the planar dimensions of the specimen, the axis-symmetry model can be adopted to analyze the local heating process with the beam center being the axis, as shown in Figure 3.

After the Fourier's law of conduction, the equation describing the heat transfer is

$$k\left(\frac{\partial^2 T}{\partial x^2}+\frac{1}{x}\frac{\partial T}{\partial x}+\frac{\partial^2 T}{\partial y^2}\right)=\rho c\frac{\partial T}{\partial t}. \tag{1}$$

The thermal boundary condition at the surface irradiated by laser is

$$-k\frac{\partial T}{\partial y}=q, \tag{2}$$

and the thermal boundary condition in the other regions of the top coat surface is

$$k\frac{\partial T}{\partial y}=h(T_e-T). \tag{3}$$

The thermal boundary condition at the cooled surface of the substrate is

$$k\frac{\partial T}{\partial y}=h(T_c-T), \tag{4}$$

where T represents temperature of the materials, ρ is density, c specific thermal capacity, q heat flux, k heat conductivity, h heat transfer coefficient between the solid surface and the cooling liquid, T_e ambient temperature (25°C), and T_c temperature of the cooling water (10°C).

Due to the fact that the order of magnitude of the loading time is 10–100 s, the equilibrium equation can be written by disregarding the effects of both coupling and inertia as

$$\frac{\partial\sigma_x}{\partial x}+\frac{\partial\tau_{xy}}{\partial y}+\frac{\sigma_x-\sigma_\theta}{x}=0, \tag{5}$$

$$\frac{\partial\sigma_y}{\partial y}+\frac{\partial\tau_{xy}}{\partial x}+\frac{\tau_{xy}}{x}=0. \tag{6}$$

The strain-displacement relations (geometry equation) are

$$[\varepsilon_x,\varepsilon_y,\varepsilon_\theta,\gamma_{xy}]^{\mathrm{T}}=\left[\frac{\partial u}{\partial x},\frac{\partial v}{\partial y},\frac{v}{r},\frac{\partial v}{\partial x}+\frac{\partial u}{\partial y}\right]^{\mathrm{T}}. \tag{7}$$

The thermo-elastical stress-strain relations (constitutive equation) are

$$\begin{aligned}&[\varepsilon_x-\varepsilon_{x0},\varepsilon_y-\varepsilon_{y0},\varepsilon_\theta-\varepsilon_{\theta0},\gamma_{xy}]^{\mathrm{T}}\\&=\left[\frac{\sigma_x-\mu(\sigma_y+\sigma_\theta)}{E},\frac{\sigma_y-\mu(\sigma_x+\sigma_\theta)}{E},\right.\\&\left.\frac{\sigma_\theta-\mu(\sigma_x+\sigma_y)}{E},\frac{2(1+\mu)\tau_y}{E}\right]^{\mathrm{T}},\end{aligned} \tag{8}$$

where $[\varepsilon_{x0},\varepsilon_{y0},\varepsilon_{\theta0}]^{\mathrm{T}}=[\alpha\Delta T,\alpha\Delta T,\alpha\Delta T]^{\mathrm{T}}$ with α being the thermal expansion coefficient.

The thermo-elastic-plastic stress-strain relations (constitutive equation) are [7, 8]

$$\begin{aligned}&[\dot\varepsilon_x-\alpha\dot T,\dot\varepsilon_y-\alpha\dot T,\dot\varepsilon_\theta-\alpha\dot T,\dot\gamma_{xy}]^{\mathrm{T}}\\&=\left[\frac{1}{E}\dot\sigma_x+\lambda\left(\sigma_x-\frac{\bar\sigma}{3}\right),\ \frac{1}{E}\dot\sigma_y+\lambda\left(\sigma_y-\frac{\bar\sigma}{3}\right),\right.\\&\left.\frac{1}{E}\dot\sigma_\theta+\lambda\left(\sigma_\theta-\frac{\bar\sigma}{3}\right),\ \frac{1+\nu}{E}\dot\tau_{xy}+\lambda\tau_{xy}\right]^{\mathrm{T}},\end{aligned} \tag{9}$$

where the superscript dot represents the increment of some variable, $\bar\sigma$ is the first stress invariable and $\lambda=\frac{E\nu}{(1+\nu)(1-2\nu)}$ with E and ν being the elastic modulus and Poisson's ratio, respectively.

The analytical solutions for such thermo-elatic-plastic problem are hard to approach, thus the numerical solutions were computed by finite element method for the temperature, deformation and stress fields of the specimen.

3.2 Numerical modeling and computation results

The thermo-mechanical performance parameters were listed in Table 1 for typical temperature points, in which symbol T represents the top coat, B the bond coat and S the substrate. Symbol ρ represents density, c is the specific thermal capacity, k thermal conductivity, α thermal expansion coefficien, E elastical modulus, υ Poisson's ratio, and σ_s yielding stress. It should be noted that fully elastic behavior was assumed for the top coat while elasto-plastic deformations were included for the bond coat and the substrate.

The axis-symmetry finite element model is shown in Figure 3, in which the Y axis represents the symmetrical axis, X axis coincides with the radial direction, Z axis the

Table 1 Thermo-mechanical parameters [9–11]

	20°C			600°C			1200°C		
	T	B	S	T	B	S	T	B	S
ρ (kg/m^3)	3470	7000	8440	3470	7000	8440	3470	7000	8440
c (J/kgK)	400	530	530	520	562	562	590	667	667
k (W/mK)	1–2	11.8	10.1	1–2	20.1	18.4	1–2	27.5	23.5
α (10^{-6}/K)	10	12.2	11.25	10	13.2	13.68	10	15.2	15.97
E (GPa)	25–35	200	208	25–35	179	187	25–35	124	148
υ	0.33	0.23	0.3	0.33	0.23	0.3	0.33	0.23	0.3
σ_s (MPa)	-	615	615	-	475	475	-	250	250

circumference direction. The top coat, bond coat and substrate are described geometrically via a tri-layer structure, of which the thermo-mechanical continuous conditions are fulfilled at every interface. In detail, the temperature and thermal flux are continuous at the interface for the heat transfer computation, while the displacement and interface stresses are continuous at the interface for the structural computation.

Due to the fact that the coupling effect is rather small, the influence of the deformation on the temperature of the materials is neglectable [8]. Thus, the temperature and deformation can be computed in sequence without considering the effect of the deformation on the heat transfer. That is, the temperature is solved firstly for the structures at certain time points. Later on, the deformations are computed for every time point by treating the node temperature as body loading. Finally, the stresses, especially the interface stresses, are obtained by solving both the geometry equation and constitutive equation. This computation was conducted by the commercial finite element software ANSYS-MULTIPHYSICS with considering the material nonlinear behavior, in particular the dependences of the thermo-mechanical performances of the materials on temperature.

The typical temperature profile is shown in Figure 4, where the temperature of the top coat surface was almost uniform along the radial direction within the region covered by the laser beam except for a little drift around the edge. Such temperature profile indicates that such local heating can provide a roughly even thermal boundary condition within the heated region.

The temperature histories of three cases with different thermal conductivities of the top coat were computed to

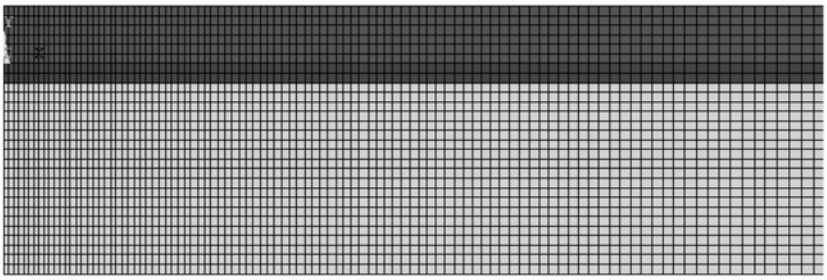

Figure 3 Sketch of the finite element model.

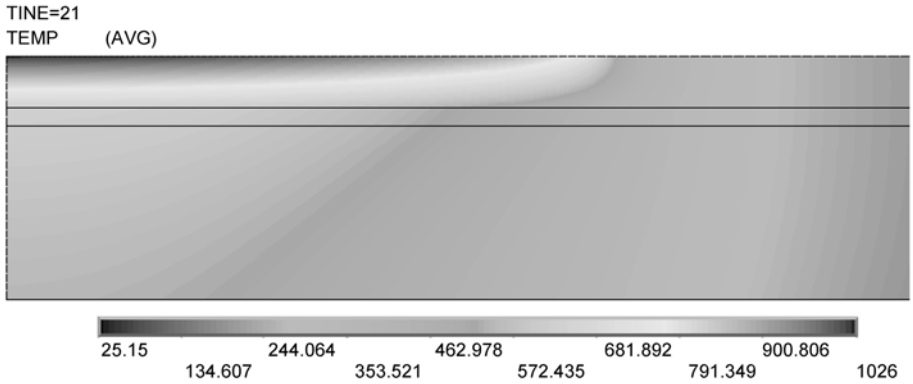

Figure 4 Temperature profile at a typical time point (t = 21 s).

investigate the effect of thermal conductivity of the top coat on heat transfer. And the temperature histories of the two nodes, i.e., the one coincided with the center point at the surface of the top coat and the center point at the interface between the top coat and bond coat, were plotted in Figures 5(a) and (b), respectively. The curves plotted in Figures 5(a) and (b) showed that the temperatures of the structure in each case achieved the steady state with the maximum value after being loaded no longer than 21 s. Thus, the results at time point t = 21 s can be used in comparison to investigate the influences of various parameters.

Moreover, the results plotted in Figures 5(a) and (b) also showed that the temperature at the surface of top coat increased obviously, while as the temperature at the interface between the top coat and bond coat hardly changed with decreasing the thermal conductivity of the top coat. This indicates that the attempt to reduce the service temperature of the bond coat via altering the thermal conductivity of the top coat is not much promising for such loading test.

The deformation of the strusture was shown in Figure 6, which reveals a hunch like deflection to the surface of the top coat due to the larger thermal expansion of the top coat in comparison to that of the bond coat and substrate. This ought to be induced by high temperature gradient through the thickness of the specimen. Such deformation gradient should inevitably be accompanied with great interfacial stresses, especially interfacial tensile stresses.

The stress component SY normal to the interface was shown in Figure 7, which confirms great interfacial tensile stresses within the region covered by the laser beam. By mapping the interfacial stresses onto the path along the interface between the top coat and the bond coat, the spatial profile of the interfacial normal stress and shear stress for time point t = 21 s were plotted in Figure 8. It was shown that there was a great interfacial tensile stress while a small shear stress at the interface. Considering the fact that the shear strength of the interface is generally greater than its tensile strength, the tensile fracture, i.e., open cracking, should dominate at the interface between the top coat and bond coat under this local heating test.

To invesitigate the temporal profile of the interfacial stresses, the evolvements of the interfacial normal stresses versus time were plotted in Figure 9 for two nodes at the interface, of which one was coincided with the center point while the other one with the point 1/2 beam radius away from the center. The results shown in Figure 9 indicated that the interfacial stresses had also approached to a steady state before 21 s, which was in agreement with the history of the

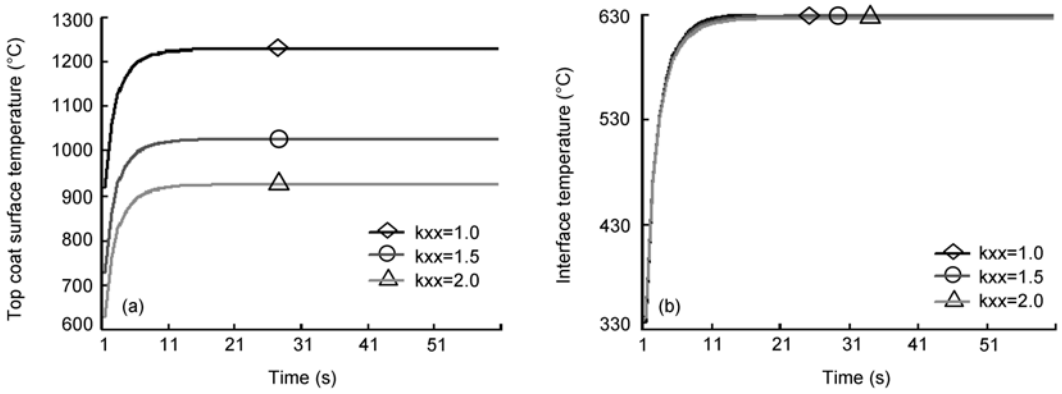

Figure 5 Dependences of (a) surface and (b) interface temperature on the thermal conductivity of top coat.

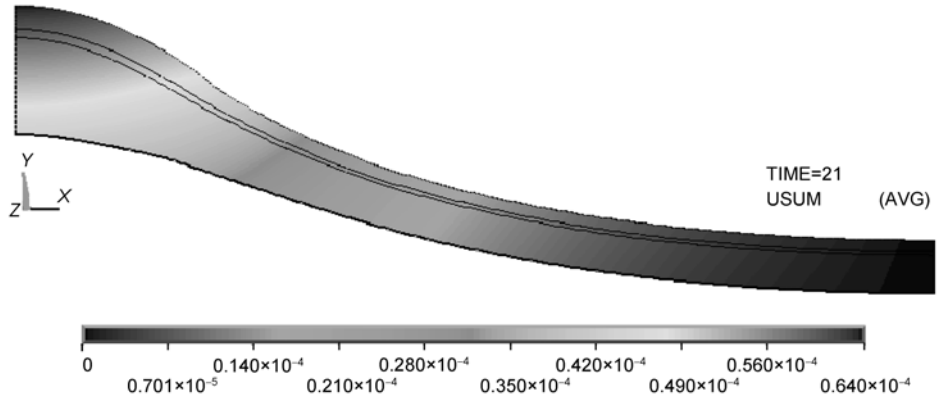

Figure 6 Typical deformation field (magnified by 100 times).

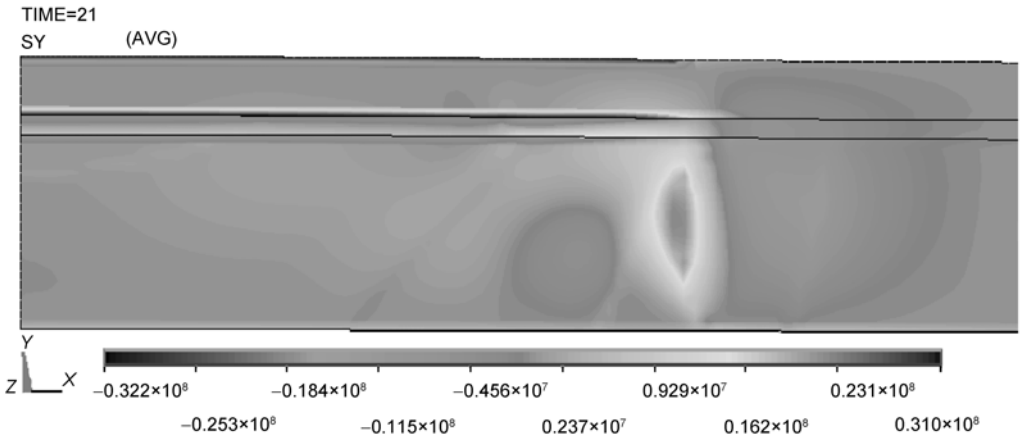

Figure 7 The stress component SY normal to the interface.

temperature. Thus, it is reasonable to compare the interfacial stresses at the time point of t = 21 s to investigate the effect of various thermo-mechanical parameters. As a matter of fact, it was also proved by computational results that the interfacial stresses at time point t = 21 s were the respective maximums for each case.

Considering that the thermal conductivity and elastic modulus of the top (ceramic) coat can be tuned via changing its porosity rate, the dependences of the peak interfacial stresses on the thermal conductivity and elastic modulus of the top coat were investigated. The results were displayed in Figure 10, in which the nine cases of three different elastic moduli (25, 30 and 35 GPa) combined with three thermal conductivities (1.0, 1.5 and 2.0 W/mK) were listed in the table at the upper-right corner. And the abscissa represented the sequence number of the cases and the ordinate was the maximum of the interfacial stress for each case. It was shown that the peak interfacial stress decreased with increasing the thermal conductivity and decreasing the elastic modulus. Moreover, it was reported that the higher porosity rate shall reduce both the thermal conductivity of the ceramic coat and its elastic modulus [4, 7]. Thus, as far as the interfacial stresses are concerned, perhaps there is a optimization value for the porosity rate of the top (ceramic) coat.

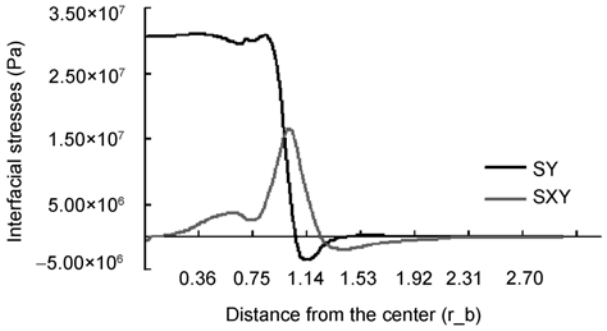

Figure 8 Spatial profile of the interfacial stresses (for t=21 s).

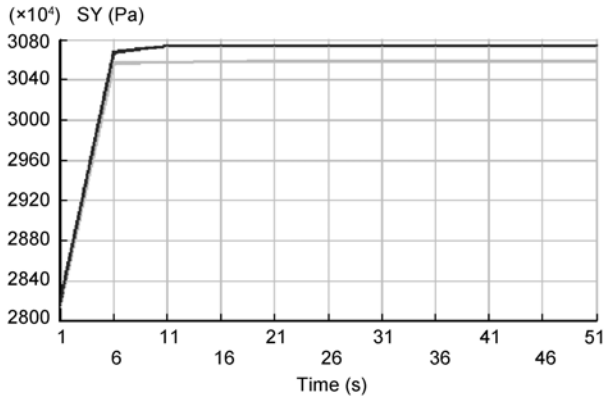

Figure 9 The histories of the interfacial normal stresses for the tow nodes.

4 Conclusions

1) The deformation mismatch between the top coat and bond coat shall be accompanied with large interfacial tensile stresses when the substrate is cooled while the top coat is subjected to local heating. Such interfacial tensile stress should lead to the interface delamination, as verified by the experimental results.

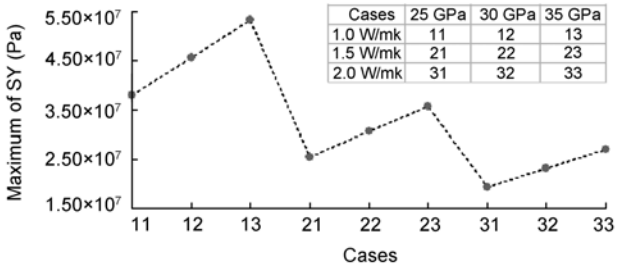

Figure 10 Dependences of the peak interfacial stresses on the thermo-mechanical parameters.

2) The main driving force of the inteface fracture, i.e.,the interfacial tensile stress, can be reduced by increasing the thermal conductivity of the ceramic coat or decreasing its elastic modulus.

This work was supported by the National Natural Science Foundation of China (Grant No. 11002145).

1 Mercier R A, McClinton C. Hypersonic propulsion–transforming the future of flight. AIAA 2003-2732, AIAA/ICAS International Air and Space Symposium, Dayton, Ohio, 2003
2 Joseph M H, James S M, Richard C M. The X-51A scramjet engine flight demonstration program. AIAA 2008-2540, 15th AIAA International Space Planes and Hypersonic Systems and Technologies Conference, Dayton, Ohio, 2008
3 Gao Z X, Lee C H. A numerical study of turbulent combustion characteristics in a combustion chamber of a scramjet engine. Sci China Ser E-Tech Sci, 2010, 40: 929–939
4 Vermaak N, Valdevit L, Evans A G. Materials property profiles for actively cooled panels: An illustration for scramjet applications. Metall Mater Trans A, 2009, 40: 877–890
5 Clarke D R, Levi C G. Materials design for the next generation thermal barrier coatings. Annu Rev Mater Res, 2003, 33: 383–417
6 Li M H, Hu W Y, Sun X F, et al. Recent research progress in thermal barrier coatings (in Chinese). Mater Rev, 2005, 19: 41–45
7 Tanigawa Y, Akai T, Kawamura R, et al. Transient heat conduction and thermal stress problems of a nonhomogeneous plate with temperature-dependent material properties. J Therm Stresses, 1996, 19: 77–102
8 Bruno A B, Jerome H W. Theory of Thermal Stresses. New York: John Wiley & Sons, 1960. 525–535
9 Sung R C, Zhu D M, Robert A M. Mechanical properties of plasma-sprayed ZrO_2-8wt% Y_2O_3 thermal barrier coatings. NASA, 2004, 213216: 1–18
10 Editorial committee for “China Aeronautical Materials Handbook”. China Aeronautical Materials Handbook (Vol. 2). Beijing: Standards Press of China, 2002. 215–223
11 Editorial committee for “China Aeronautical Materials Handbook”. China Aeronautical Materials Handbook (Vol. 9). Beijing: Standards Press of China, 2002. 333–340